Newport Beach, CA, USA
ACTIVE 95
1995 July 06–08

GLOBAL ACTIVE NOISE CONTROL IN RECTANGULAR ENCLOSURES

Scott D. Sommerfeldt, John W. Parkins, and Young C. Park

Graduate Program in Acoustics
The Pennsylvania State University
State College, PA 16804

INTRODUCTION

There are a number of problems in active noise control that involve the need to achieve global control, or at least control over an extended region, of the sound field in an enclosure. The approach generally used in the past has been to minimize the pressure at a large number of error sensors distributed throughout the enclosure. An alternative approach, based on minimizing the acoustic energy density at an error sensor location, has been developed in recent years[1,2]. The method has been tested both numerically and experimentally in one-dimensional enclosures, and has also been tested numerically for a three-dimensional enclosure. These results have indicated that one can often achieve improved global attenuation by minimizing the acoustic energy density, rather than the squared pressure signal. It has also been found previously that there is much less dependence in the performance of the active control system on the error sensor locations, since the energy density has fewer nodal surfaces than the pressure. This characteristic has important implications for applications where the choices for error sensor locations may be limited.

In this paper, preliminary experimental results are presented to compare the performance achieved by minimizing either the acoustic energy density or the squared pressure. In the case of minimizing the energy density, it is necessary to sense not only the pressure but also the three velocity components. The sensor developed to accomplish this task is described, and some active control results obtained are presented. These results are obtained by minimizing either the energy density or the squared pressure at the error sensor location, and scanning the acoustic field using an independent microphone. This allows one to map the acoustic field throughout the enclosure and estimate the resulting global potential energy with the two control approaches. The trends observed experimentally are in accordance with expectations, and indicate that controlling energy density has the potential to achieve greater global control than controlling the squared pressure.

CONTROL IMPLEMENTATIONS

The focus of the current work is to investigate the global control that can be achieved for various control implementations, given an arbitrary source and sensor configuration. As a result, there has been no attempt to optimize any of the source or sensor locations. The focus is simply to compare the performance that can be realized for a given configuration. This corresponds to the situation

that often occurs in practice, where one has limited control over the possible locations for sources and sensors. Also, for this initial experimental investigation, a single primary source, a single control source, and a single error sensor location are used to simplify the configuration. Multiple sources and sensors have been investigated numerically, and will be investigated experimentally in future work.

Three different performance functions have been investigated numerically to compare the global performance that can be achieved. The first performance function corresponds to the global potential energy in the enclosure, as suggested by Nelson, *et al.*[3] This is impractical for experimental implementation, but serves as a useful benchmark. The second performance function corresponds to the squared pressure at the sensor location, which is the control approach that has generally been implemented. It is well known that this approach often leads to localized control effects, rather than the broad global attenuation desired. In practice, this difficulty is circumvented by increasing the number of error sensors to achieve control over a broader region of the enclosure. The third performance function consists of the total acoustic energy density at the sensor location, given by $p^2/(2\rho c^2) + (1/2)\rho v^2$, where ρ is the fluid density, c is the acoustic phase speed, p is the pressure, and v is the particle velocity. This approach makes use of a local measurement, but the measurement of the energy density yields more global information than is obtained from a pressure measurement.

For the experimental work reported here, two of the control schemes mentioned have been implemented. These two approaches consist of minimizing the squared pressure and minimizing the energy density at the error sensor location. In both cases, the quantity of interest is minimized by means of an adaptive filtered-x algorithm. The form of this algorithm for minimizing the squared pressure is well known[4], and the recursion for updating the control filter coefficients is given by

$$w_i(n+1) = w_i(n) - \mu e(n) r(n-i) \ . \tag{1}$$

Here, $w_i(n)$ represents the ith coefficient of the control filter at discrete time n, μ is a convergence parameter chosen to maintain stability, $e(n)$ is the error signal (pressure) measured at the error microphone, and $r(n)$ is the filtered reference signal, obtained by passing the reference input signal through the transfer function from the controller output to the error sensor input. The filtered-x algorithm can also be used to minimize the acoustic energy density. In this case, the appropriate recursion for updating the control filter coefficients is given by[1]

$$w_i(n+1) = w_i(n) - \mu \left(\sum_{m=1}^{3} \rho v_m(n) r_{vm}(n-i) + \frac{1}{\rho c^2} p(n) r_p(n-i) \right) \ . \tag{2}$$

In this equation, $m = 1,2,3$ corresponds to the x-, y-, z-direction, respectively, v_m is the velocity in the m direction, $r_{vm}(n)$ is the filtered reference signal obtained by passing the reference input signal through the transfer function from the controller output to the velocity component in the m direction at the error sensor, and $r_p(n)$ is the filtered reference signal obtained by passing the reference input signal through the transfer function from the controller output to the pressure at the error sensor.

It can be seen from Eq. (2) that minimizing the energy density requires not only the measurement of the pressure at the error sensor, but also the measurement of all three orthogonal velocity components at the error sensor. In addition, in the full implementation it is also necessary to model the transfer functions from not only the controller to the pressure at the error sensor, but also from the controller to each velocity component at the error sensor. Both control implementations

described above have been implemented on a Spectrum 96002 System Board. For both control approaches, the transfer functions required to obtain the filtered reference signals are adaptively estimated in real-time using a passive system identification procedure reported previously[5]. For the case of controlling the energy density with a single source and sensor, there are four transfer functions required for the filtered reference signals, in addition to recursively updating the control filter.

ENERGY DENSITY SENSOR

From Eq. (2), it is apparent that each component of the acoustic particle velocity must be measured for proper implementation of the control algorithm. This was accomplished by using finite differences with two closely spaced microphones in each direction. This follows directly from Euler's equation, given as

$$v_m(n) = \frac{-1}{\rho}\int \frac{\partial p}{\partial x_m}\,dn \approx \frac{-1}{\rho\,\Delta x_m}\int \left[p_2(n) - p_1(n)\right] dn \quad , \tag{3}$$

where Δx_m is the spacing between two closely spaced microphones in the x_m direction.

It was desired to develop a relatively inexpensive probe to measure the energy density. This was accomplished using six Lectret 1207A microphones that were flush mounted in a 5.1 cm wooden ball, as shown in Figure 1. The three pairs of microphones were mounted on opposite sides of the sphere, so as to be able to estimate the three orthogonal components of the particle velocity. This type of spherical probe has been discussed previously by Elko[6], and was shown to have favorable characteristics with respect to the finite difference and finite sum bias errors. The inside of the wooden ball was hollowed out, and a small circuit board was mounted inside the ball. Six noninverting pre-amplifiers were mounted on the circuit board to buffer the outputs from the microphone and to provide voltage gain. The amplified signals from the six microphones are

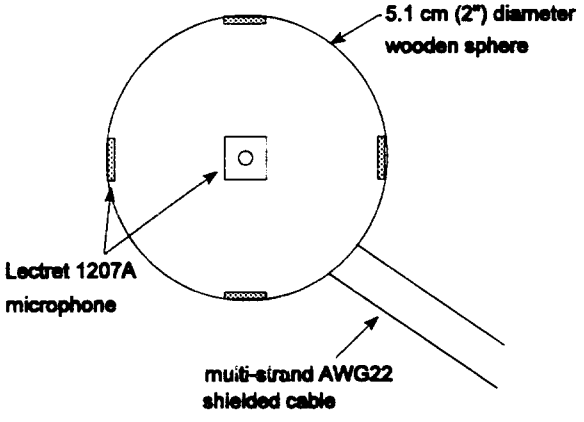

Figure 1. Schematic of the energy density sensor probe.

transmitted by means of a shielded cable to a second set of noninverting amplifiers located outside of the enclosure. These amplifiers have variable resistors associated with them that allow the gains of the amplifiers to be adjusted for microphone calibration purposes.

Each of the six microphones was calibrated by placing each microphone into one side of a small calibration chamber, along with a B&K Type 4133 microphone, as shown in Figure 2. The gain for the microphone was then adjusted so that the output level was 50 dB higher than that of the B&K microphone. The result of this process was that the microphones were all calibrated to provide an output of 1 Vrms @ 94 dB re 20μPa at 100 Hz. The Lectret microphones were found to provide a stable, linear response up to levels greater than 110 dB re 20μPa, with a flat phase and amplitude response. The phase response is within ±1° at 100 Hz for all six microphones, and is within that range for all frequencies of interest above 100 Hz.

With the energy density probe, the three pairs of microphones could be used to provide the finite difference estimation of the pressure gradient in Eq. 3. To obtain the velocity components, it is also necessary to perform a time integration of the pressure difference. This has been done both digitally and with an analog circuit. For the results presented here, a digital integration scheme was implemented, in accordance with the work presented by Hodges, *et al.*[7] With this approach, the six microphones are input to the DSP board, where the average of the six pressure signals is used as an estimate of the pressure at the sensor location, and the time integration of the pressure differences in each direction is used to obtain the particle velocity components, as given in Eq. 3.

EXPERIMENTAL CONFIGURATION

The two control implementations described previously were tested in a rectangular enclosure with internal dimensions 1.93 m × 1.22 m × 1.54 m. The walls were constructed of 19 mm thick plywood, and were reinforced on the exterior surfaces to reduce the vibration of the walls. For the results presented here, a single Bose 101 loudspeaker was used as the primary source and a second Bose 101 loudspeaker was used as the control source. The primary source was located at the position (0.15, 0.22, 0.07) m and the secondary source was located at the position (1.78, 0.22, 0.07) m. The sound field was controlled by minimizing either the squared pressure or the energy density at the error sensor location.

A B&K Type 4133 microphone was mounted on a traversing system that could be used to

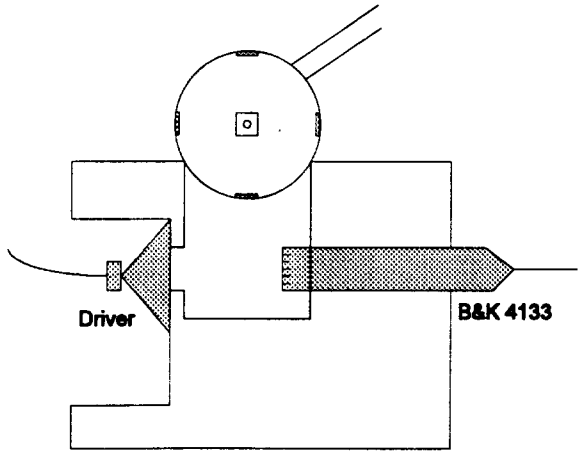

Figure 2. Calibration chamber used to calibrate the energy density probe.

manually scan a horizontal plane in the enclosure. After convergence of the controller, the pressure field was scanned over five horizontal planes to obtain an estimate of the global characteristics of the acoustic field. Each of the five horizontal planes was separated by a distance of 25 cm. The grid spacing of the measurement points in the horizontal plane corresponded to 10 cm in the x-direction (1.93 m) and 11 cm in the y-direction (1.22 m). It should be noted that due to the nature of the traversing system it was not possible to obtain measurements over the three grid points closest to the walls in the x-direction. As a result, there were thirteen grid points in the x-direction, eleven grid points in the y-direction, and five grid points in the z-direction, for a total of 715 measurements for each control condition. These measurements were made for the case of no control, as well as for the cases of squared pressure and energy density control.

EXPERIMENTAL RESULTS

To determine how the response of the experimental enclosure compared with the numerical enclosure studies previously, one of the loudspeakers was placed in a corner of the enclosure, and a microphone was placed in another corner to measure the frequency response of the enclosure. The experimental response is shown in Figure 3. The resonance frequencies of the enclosure are in good agreement with the numerical predications, as can be seen in Table 1. There are some additionalspectral peaks, for example at 51, 56.5, 147.5, 159, and 189 Hz, that do not match up with predicted frequencies. It is thought that these frequencies are associated with resonance frequencies of the enclosure walls, which are not completely rigid.

For this preliminary investigation, the two control schemes were each implemented and the acoustic field was scanned over the five horizontal planes. The results were then compared with the predicted results obtained from the numerical model to compare the spatial dependence of the field and the overall attenuation levels achieved. Several of the results obtained will be discussed here.

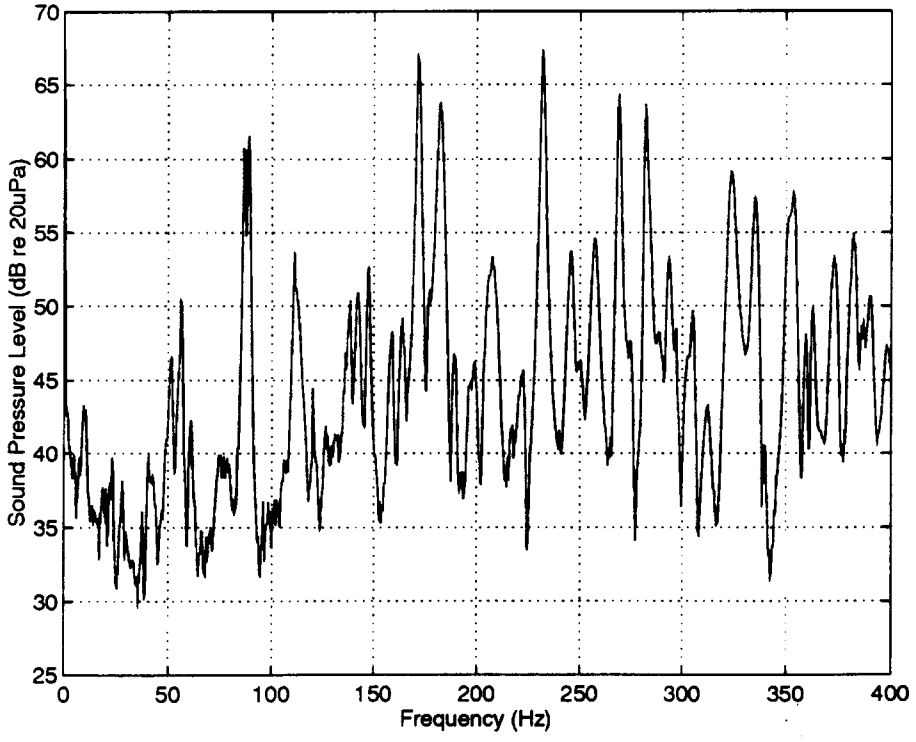

Figure 3. Measured frequency response of the enclosure.

Table 1. Numerical vs. Experimental Resonance Frequencies for the Enclosure.

Mode Number	Numerical Frequency (Hz)	Experimental Frequency (Hz)
(1,0,0)	88.9	88
(0,0,1)	111.4	111
(0,1,0)	140.6	139
(1,0,1)	142.5	142
(1,1,0)	166.3	170
(2,0,0)	177.7	182.5
(0,1,1)	179.3	182.5
(1,1,1)	200.1	199
(2,0,1)	209.7	207.5

Some of the results obtained for an excitation frequency of 88 Hz (1,0,0 mode) can be seen in Figures 4-7. These figures show both the numerical and experimental results for two of the five horizontal planes that were scanned. For the numerical results, the pressure field was determined for the cases of no control, controlling the squared pressure, controlling the energy density, and controlling the global potential energy. For these results, the error sensor was located at (0.96, 0.19, 0.76) m. This location represents a poor choice for the error sensor location when controlling the squared pressure, since it is located very near to the nodal plane for the (1,0,0) mode. As a result, the dominant mode in the enclosure is not observed by the control system, and the overall levels in the enclosure go up when the control is implemented, even though the local pressure at the error sensor is attenuated. This effect is apparent in both the numerical and the experimental results. On the other hand, when the energy density is controlled, the energy density does not have a node at the error sensor location. As a result, the controller is able to sense the dominant mode in the enclosure without difficulty and achieve a global control effect. It can be observed from Figures 4-7 that the general agreement for the spatial dependence of the field is quite good. The effect of controlling the energy density for this frequency is to yield a pressure field that is relatively uniform throughout the enclosure, and at a lower level than the uncontrolled field. It can also be seen from the numerical predictions that the energy density control closely approximates the control that would be achieved if one could minimize the global potential energy in the enclosure.

Figures 8-11 show the numerical and experimental results obtained for two of the five horizontal planes scanned with an excitation frequency of 170 Hz (166.3 Hz numerically). This frequency corresponds to the (1,1,0) mode. For these results, the error sensor was located at (0.625, 0.615, 0.775) m. This location again represents a poor error sensor location for controlling the squared pressure, since it is located near the nodal plane at $y = 0.61$ m. As a result, the controller is not able to observe the dominant mode when minimizing the squared pressure, and local attenuation at the error sensor results with the level of the dominant (1,1,0) mode increasing throughout the enclosure. On the other hand, when the energy density is minimized, the error sensor is able to sense the dominant mode and attenuate its amplitude throughout the enclosure. It can be seen from Figures 8 and 9 for the $z = 0.25$ m plane that the residual acoustic field closely resembles the (2,0,0) mode, which can be seen from Table 1 to be the residual mode whose resonance frequency is closest to the excitation frequency of 170 Hz. It can again be seen that there is reasonable agreement between the spatial dependence obtained experimentally and the spatial dependence predicted numerically.

The global potential energy in the enclosure can be determined by integrating the squared

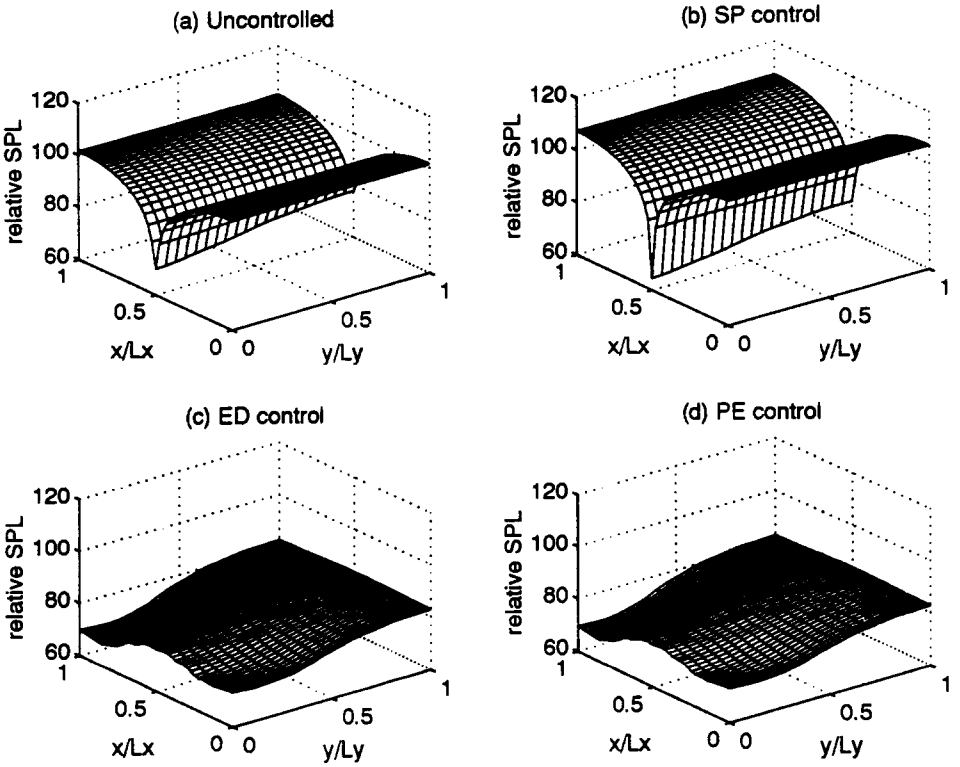

Figure 4. Predicted sound pressure distribution for the plane z = 0.76 m. (88.9 Hz - (1,0,0) mode).

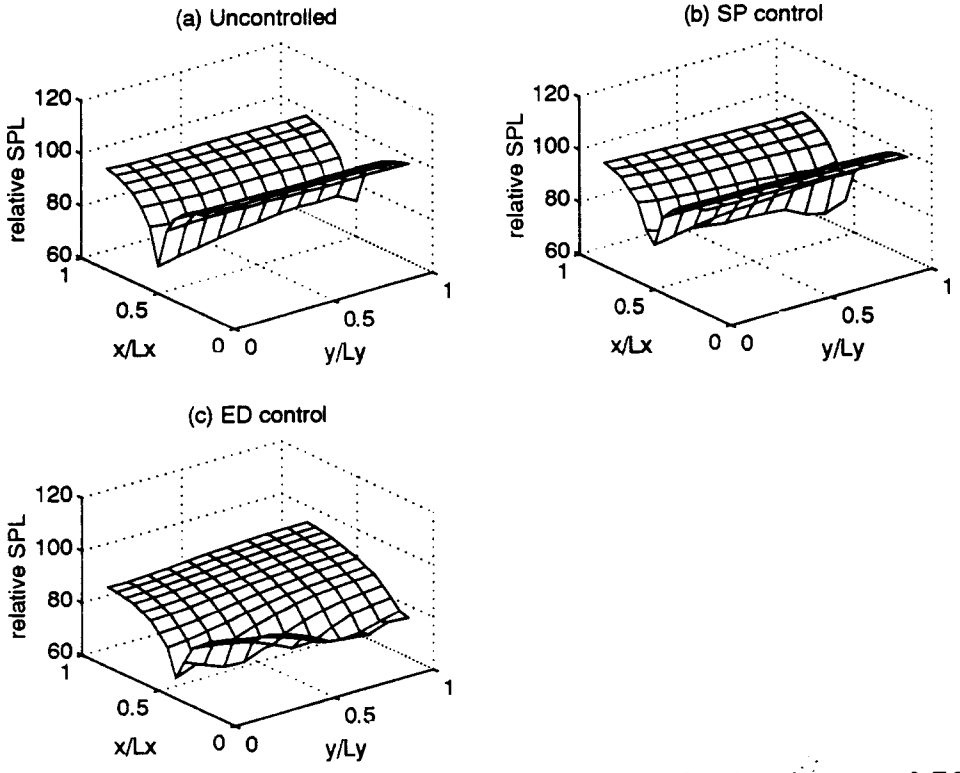

Figure 5. Experimental sound pressure distribution for the plane z = 0.76 m. (88 Hz - (1,0,0) mode).

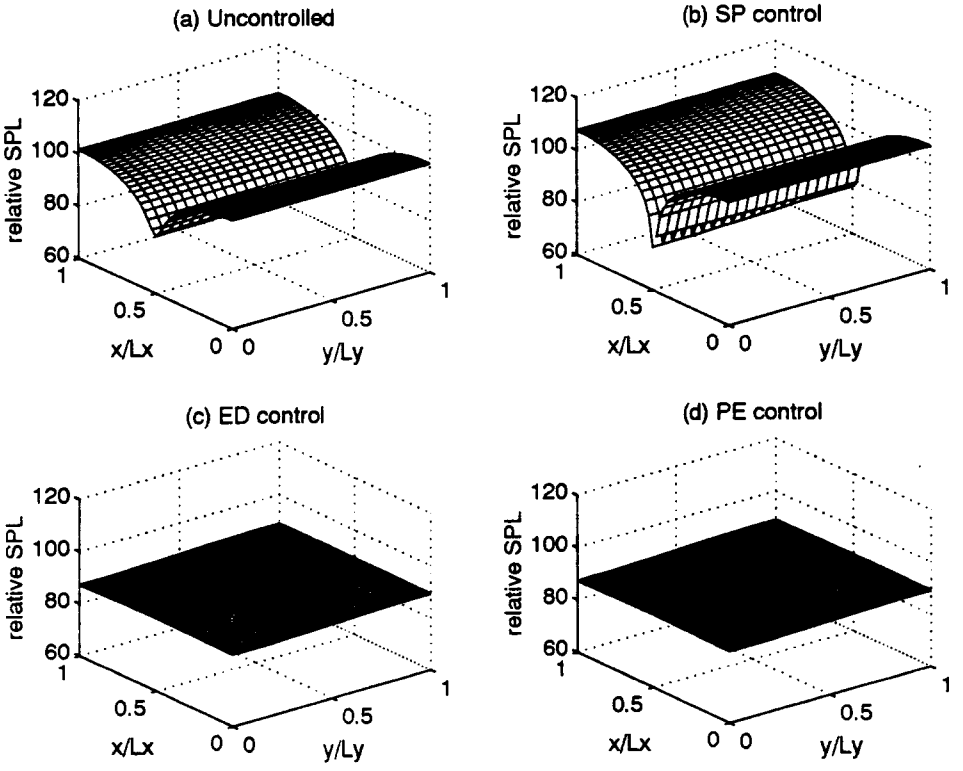

Figure 6. Predicted sound pressure distribution for the plane z = 1.28 m. (88.9 Hz - (1,0,0) mode).

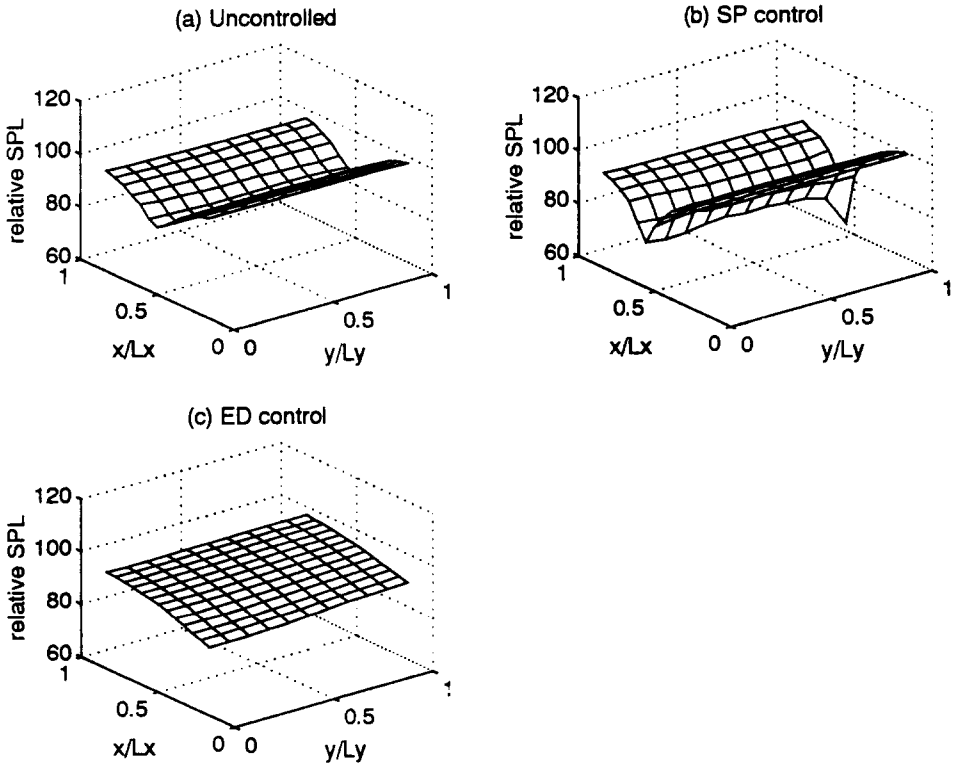

Figure 7. Experimental sound pressure distribution for the plane z = 1.28 m. (88 Hz - (1,0,0) mode).

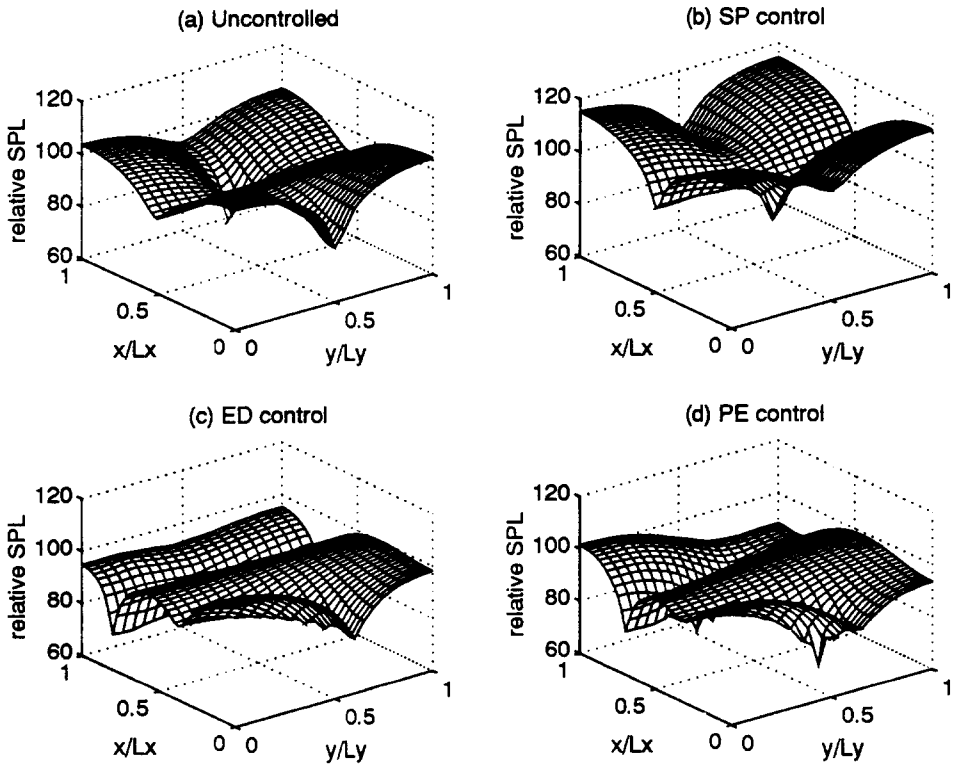

Figure 8. Predicted sound pressure distribution for the plane z = 0.25 m. (166.3 Hz - (1,1,0) mode).

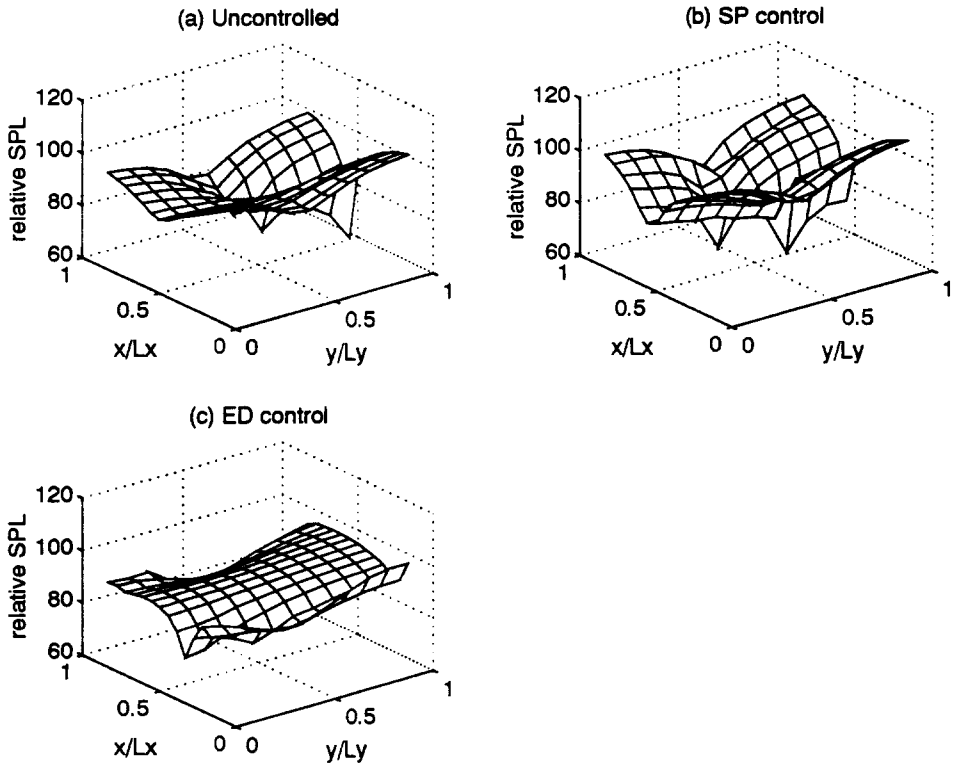

Figure 9. Experimental sound pressure distribution for the plane z = 0.25 m. (170 Hz - (1,1,0) mode).

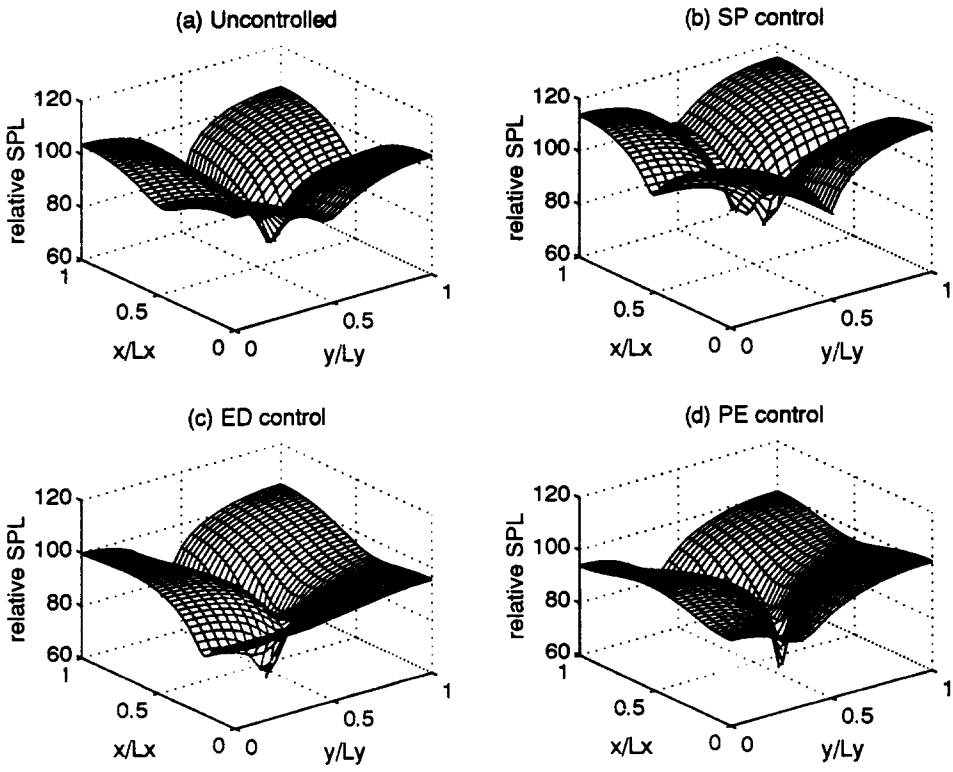

Figure 10. Predicted sound pressure distribution for the plane z = 1.28 m. (166.3 Hz - (1,1,0) mode).

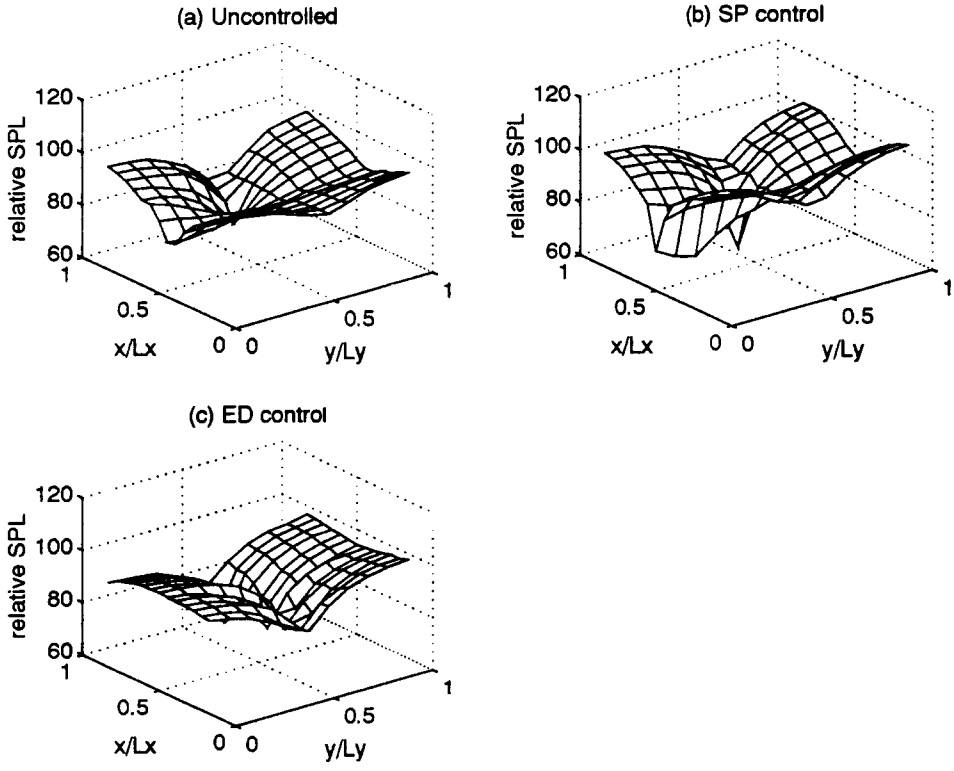

Figure 11. Experimental sound pressure distribution for the plane z = 1.28 m. (170 Hz - (1,1,0) mode).

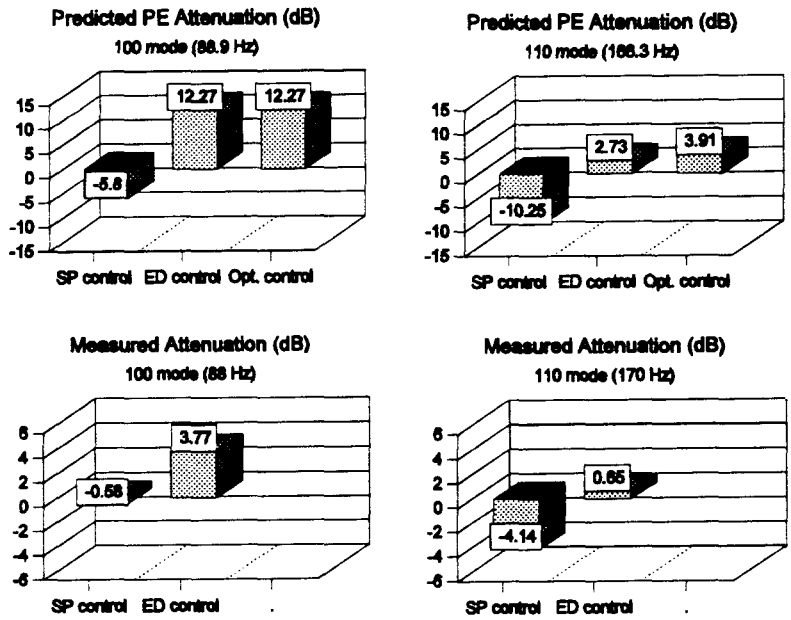

Figure 12. Predicted and measured attenuations of the global potential energy.

pressure over the volume of the enclosure. For the case of the experimental results, this was approximated by summing up the squared pressures from all of the measurement grid points, as

$$E_p(dB) = 10 \log_{10}\left(\sum_{ix=1}^{13} \sum_{iy=1}^{11} \sum_{iz=1}^{5} p^2(ix,iy,iz)\, dx\, dy\, dz \right), \tag{4}$$

where $dx = 0.1$ m, $dy = 0.11$ m, and $dz = 0.25$ m. The results are shown in Table 2 for the (1,0,0) and (1,1,0) modes, and the attenuation of the potential energy achieved is shown in Figure 12. For

Table 2. Potential Energy (dB) in the Enclosure With and Without Control.

	Uncontrolled	Squared Press. Control	Energy Density Control	Potential Energy Control
Numerical:				
(1,0,0) mode (88.9 Hz)	12.6	18.4	0.3	0.3
(1,1,0) mode (166.3 Hz)	12.3	22.6	9.6	8.4
Experimental:				
(1,0,0) mode (88 Hz)	3.1	3.9	-0.1	
(1,1,0) mode (170 Hz)	2.7	7.0	1.4	

the numerical results, the attenuation in the potential energy is shown for minimizing the squared pressure, the energy density, and the potential energy. For the experimental results, the attenuation is shown for controlling the squared pressure and the energy density. It can be seen that the predicted trends are observed experimentally in both cases. The attenuation achieved when controlling energy density and the amplification achieved when controlling the squared pressure is not as large as predicted. It is thought that this may in part be due to the missing grid points along the x-axis, due to the nature of the traversing mechanism. The largest reductions would be expected to occur near the walls of the enclosure, so that these missing points could lead to the results observed. Nonetheless, the results do demonstrate that for these cases the minimization of energy density leads to significantly improved global control of the acoustic field.

CONCLUSIONS

A filtered-x adaptive feedforward control system has been developed that is capable of minimizing either the squared pressure or the energy density at one or more sensor locations. A low cost three-dimensional energy-density probe has been developed and tested for proper measurement characteristics. Preliminary experimental results have been obtained for comparison with previous numerical work, and some of those results presented here. The modes chosen here were chosen as cases where numerical predictions indicated significantly improved attenuation should be achieved by controlling the energy density. The experimental results confirmed the proper trends expected, and give confidence in the earlier numerical results. The numerical results have indicated that minimizing energy density is generally preferable for achieving global control of the field.

The experimental work will be expanded to look at more complex acoustic fields and to investigate the effect of using multiple sources and/or sensors. These results can then be used to verify previous numerical work. In addition, the sensitivity of the energy density control approach to error sensor location will be further studied experimentally to verify its relative insensitivity to location.

ACKNOWLEDGEMENT

The authors gratefully acknowledge the support of this work by NASA Langley Research Center under NASA Grant NAG-1-1557.

REFERENCES

1. "An adaptive filtered-x algorithm for energy-based active control," S. D. Sommerfeldt and P. J. Nashif, *J. Acoust. Soc. Am.*, **96**, 300-306 (1994).
2. "An evaluation of active noise attenuation in rectangular enclosures," S. D. Sommerfeldt and J. W. Parkins, *Proc. Inter-Noise 94*, 1351-1356 (1994).
3. "The active minimisation of harmonic enclosed sound fields," P. A. Nelson, A. R. D. Curtis, S. J. Elliott, and A. J. Bullmore, *J. Sound Vib.*, **117**, 1-58 (1987).
4. B. Widrow and S. D. Stearns, *Adaptive Signal Processing* (Prentice-Hall, Englewood Cliffs, NJ, 1985).
5. "Multi-channel adaptive control of structural vibration," S. D. Sommerfeldt, *Noise Control Eng. J.*, **37**, 77-89 (1991).
6. "An acoustic vector-field probe with calculable obstacle bias," G. W. Elko, *Proc. Noise-Con 91*, 525-532 (1991).
7. "The design of a precision digital integrator for use in an active vibration control system," T. Hodges, P. A. Nelson, and S. J. Elliott, *Mech. Systems Sig. Proc.*, **4**, 345-353 (1990).